Controllers for Unicycle-Type Wheeled Robots: Theoretical Results and Experimental Validation

ByungMoon Kim and Panagiotis Tsiotras, *Senior Member, IEEE*

***Abstract*—Mobile robots offer a typical example of systems with nonholonomic constraints. Several controllers have been proposed in the literature for stabilizing these systems. However, few experimental studies have been reported comparing the characteristics and the performance of these controllers with respect to neglected dynamics, quantization, noise, delays, etc. In this paper, we use a Khepera mobile robot to perform experimental comparison of several control laws. Khepera has two dc motor-powered wheels and introduces many realistic difficulties, such as different motor dynamics for the two wheels, time delay, quantization, sensor noise, and saturation. We emphasize the implementation difficulties of two discontinuous controllers proposed herein, and we compare their performance with several other controllers reported in the literature. Ways to improve the performance of each controller are also discussed.**

***Index Terms*—Experimental results, nonholonomic systems, stabilization, tracking, wheeled robots.**

I. Introduction

AN UNDERACTUATED system is one with a smaller number of control inputs than the number of independent generalized coordinates. Often, underactuated systems arise as a result of some nonintegrable motion constraints. In such systems, it is not possible to choose generalized coordinates equal to the number of degrees of freedom (DOF). The number of generalized (i.e., Lagrangian) coordinates exceeds the number of degrees of freedom by the number of independent, nonintegrable constraints [14, p. 66]. Such systems are called nonholonomic. Several examples which involve nonholonomic constraints can be found in real-world applications, such as mobile robots, bicycles, cars, underactuated spacecraft, underwater vehicles, etc. Several approaches have been proposed for stabilizing nonholonomic systems. One such approach is to use time-varying controllers [15], [13], [11], [16], [10]. These time-varying control laws have typically slow rates of convergence [9]. Experimental validation of time-varying controllers can be found in [11]. An alternative approach is to use time-invariant, discontinuous controllers such as those in [4], [18], [8], [1], [19], [3], and [2]. These discontinuous control laws ensure exponential convergence rates. A comparative study of controllers for nonholonomic systems and, in particular, between time-varying and time-invariant controllers, has not been done, at least as far as the authors know. This is clearly of great interest. Moreover, the robustness properties of these controllers is still a topic under investigation. This paper provides a step toward this goal by comparing the stabilization and robustness properties of several time-varying and time-invariant controllers for a wheeled robot. It should be noted that a comprehensive investigation of the issues associated with the experimental implementation of controllers for mobile robots has also recently appeared in [6].

All controllers in this paper are implemented on a unicycle-type robot called Khepera. This robot has two dc motor-powered wheels and introduces many realistic difficulties, such as different motor dynamics for the two wheels, time delay, quantization, sensor noise, and saturation. The performance of each controller was tested with respect to convergence characteristics, speed of response, steady-state error, robustness to sensor noise, etc. Suggestions on how to improve each controller's performance are also presented.

The paper is organized as follows. In Section II, we present the mathematical equations used to describe the kinematics of a unicycle-type wheeled robot. Two somewhat different state and input transformations of these equations result in two slightly different implementations (herein called System I and System II) of the control laws. The effects of choosing either of these two implementations is discussed in detail later in the paper. In Section III, we present two discontinuous, time-invariant control laws. These control laws are based on the results of [19], [17], and [2]. Proper implementation of these control laws requires some care in order to avoid the singularity at the origin. Section IV summarizes the controllers tested in this work. Details for each controller can be found in the relevant references. The description of the experimental setup and the problems encountered during the implementation of these controllers are given in Section V. Sensor noise, quantization error, and motor dynamics all affected the performance of the control laws. The steps taken to reduce these effects are outlined in detail. To make a fair comparison between all controllers, several robot missions were devised. Considerable effort was devoted to finding the best gains for each controller. Section VI summarizes the experimental results. Conclusions are given in Section VII.

II. Kinematic Equations

Consider a unicycle-type robot, as shown in Fig. 1. The kinematic equations of the robot are

$$\dot{x} = v\cos\gamma \quad \dot{y} = v\sin\gamma \quad \dot{\gamma} = \omega. \tag{1}$$

Manuscript received July 13, 2001; revised March 16, 2002. This paper was recommended for publication by Associate Editor Y. Xu and Editor A. De Luca upon evaluation of the reviewers' comments. This work was supported in part by National Science Foundation Awards CMS-9996120 and INT-9996096 and by the US Army Research Office under contract DAAD19-00-1-0473.

B. Kim is with the College of Computing, Georgia Institute of Technology, Atlanta, GA 30332-0280 USA (e-mail: bmkim@cc.gatech.edu).

P. Tsiotras is with the School of Aerospace Engineering, Georgia Institute of Technology, Atlanta, GA 30332-0150 USA (e-mail: p.tsiotras@ae.gatech.edu).

Publisher Item Identifier S 1042-296X(02)05283-7.

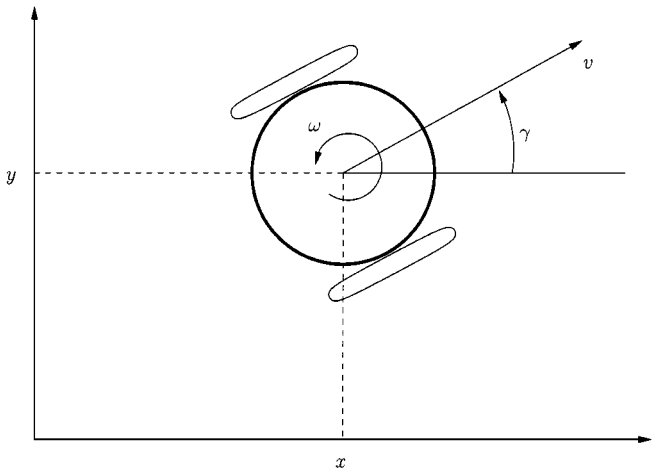

Fig. 1. Definition of configuration variables.

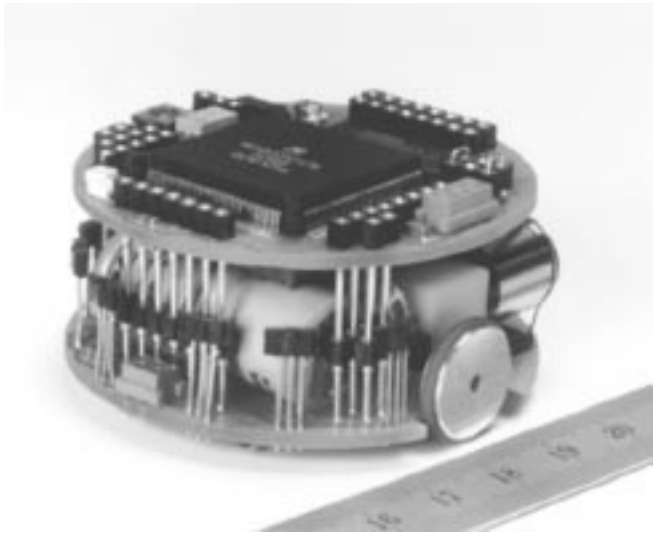

Fig. 2. Khepera robot.

The kinematic model of a differentially steered mobile robot (such as the Khepera, shown in Fig. 2) has two control inputs, the velocities of the left and right wheels, v_1 and v_2. These are related to the forward velocity v and the angular velocity ω of the robot by $v_1 = v - R\omega$, $v_2 = v + R\omega$ where R is half the distance between the two robot wheels. Therefore, the kinematics of a differentially steered mobile robot can be described by the unicycle kinematics (1). Equation (1) can be transformed to the normal chained (or power) form by a state and input transformation. Using the state transformation [5]

$$\begin{aligned} x_1 &= x\cos\gamma + y\sin\gamma \\ x_2 &= \gamma \\ x_3 &= x\sin\gamma - y\cos\gamma \end{aligned} \tag{2}$$

one arrives at two slightly different systems, depending on the input transformation used. System I is given by

$$\dot{x}_1 = u_1 \quad \dot{x}_2 = u_2 \quad \dot{x}_3 = x_1 u_2 \tag{3a}$$

$$v = u_1 + x_3 u_2 \quad \omega = u_2 \tag{3b}$$

and System II is given by

$$\dot{x}_1 = u_1 - x_3 u_2 \quad \dot{x}_2 = u_2 \quad \dot{x}_3 = x_1 u_2 \tag{4a}$$

$$v = u_1 \quad \omega = u_2. \tag{4b}$$

These two systems are completely equivalent when the inputs are the linear velocity v and the angular velocity ω. However, they are different when the inputs are u_1 and u_2. Compare (3a) and (4a). Our experimental results have shown that the extra term $x_3 u_2$ has a significant effect on the transient response of the robot. Although it is easier to design a control law using System I, our results have shown that practical implementation favors System II. This fact has also been observed by M'Closkey and Murray [11], [12] where they implemented their controllers (derived based on System I) using System II. Fortunately, it turns out that the extra term $x_3 u_2$ in (4a) does not destroy stability. Our experiments actually showed that working with System II was almost always beneficial.

III. Two Time-Invariant Controllers

In this section, we present two time-invariant, discontinuous controllers. Their derivation uses ideas from invariant manifold theory [17], [2], [8].

A. Controller 1

This controller was first proposed in [17] and uses the same ideas as in [18]. A more general version of this controller has been proposed in [2]. The control law is given by

$$u_1 = -kx_1 + \mu\frac{s(x)}{x_1^2 + x_2^2}x_2 \quad u_2 = -kx_2 - \mu\frac{s(x)}{x_1^2 + x_2^2}x_1 \tag{5}$$

where s is given by $s(x) := x_3 - (1/2)x_1x_2$. The derivative of s is readily calculated as

$$2\dot{s} = x_1u_2 - u_1x_2. \tag{6}$$

Consequently, the states $(x_1, x_2, 2s)$ correspond to the well-known nonholonomic integrator of Brockett [4], [2].

The function $s : \Re^3 \to \Re$ defines a manifold $\mathcal{M}$ in $\Re^3$ by $\mathcal{M} = \{x \in \Re^3 : s(x) = 0\}$. It can be easily shown that $\mathcal{M}$ is an invariant manifold for (3a) with control (5). Moreover, for all initial conditions $x(0) \in \mathcal{M}$, the state x decays exponentially to zero as $t \to \infty$. For initial conditions $x(0) \notin \mathcal{M}$, the control law (5) is such that $s \to 0$ with an exponential rate of convergence.

The controller given by (5) is not defined on the x_3 axis, i.e., for $x_1 = x_2 = 0$. This is a singular case and a modification of the control law in (5) around the x_3 axis is needed to avoid this singularity. Such a modification is discussed later in this section. As shown next, for all initial conditions $x_1^2(0) + x_2^2(0) \neq 0$, the system (3a) with this control law is "almost exponentially stable" [2].

Proposition 1: The control law given by (5) almost exponentially stabilizes (3a) for all initial conditions, such that $x_1(0) \neq 0$ and $x_2(0) \neq 0$, if $\mu > 0$ and $k > 0$. Moreover, if $\mu > 2k > 0$, the control inputs u_1 and u_2 are bounded along the trajectories of the closed-loop system.

Proof: See [17] or [2] . ■

Remark 1: The notion of almost exponential stability (AES) used here is the same as the one in [2]. That is, for any open and dense set Ω in $\Re^3$ AES implies: 1) existence of solutions for all $t \geq 0$ and for all initial conditions in Ω; 2) exponential convergence of the closed-loop trajectories to the origin; and 3) a Lyapunov-type stability with respect to the subspace topology induced on $\Re^3$ by Ω. Similarly to AES, one can introduce the notions of almost asymptotic stability (AAS) if 2) is replaced by asymptotic convergence to the origin. A system is locally AES (LAES) or locally AAS (LAAS) if the set Ω is bounded.

Next, we turn our attention to System II with controller (5). The next proposition basically states that the extra term $-x_3u_2$ in the $\dot{x}_1$ equation for System II does not destroy asymptotic stability.

Proposition 2: System (4a) with the control law given in (5) is LAAS, if $k > 0$ and $\mu > 0$. Moreover, if $\mu > 2k$, the control inputs are bounded along the closed-loop trajectories.

A complete proof of this result is given in the Appendix.

Singularity Avoidance: A modification of the control law (5) in a neighborhood of the x_3 axis is necessary, since this control law is not defined when $x_1 = x_2 = 0$. The modification used here is similar to the one presented in [18]. The idea is to create a region around the x_3 axis where the control law (5) is not used. To this end, let the region $\mathcal{D}_{\bar{\eta}}^b = \{(x_1, x_2, x_3): |\eta| \geq \bar{\eta}\}$ where

$$\eta := \frac{s}{\sqrt{x_1^2 + x_2^2}} = \frac{s}{\nu}. \tag{7}$$

With a slight abuse of notation, we let $\mathcal{D}_{\infty}^b$ denote the set $\mathcal{D}_{\infty}^b = \{(x_1, x_2, x_3): \nu = 0, s \neq 0\} = \{(x_1, x_2, x_3): x_1 = x_2 = 0, x_3 \neq 0\}$. In the set $\mathcal{D}_{\bar{\eta}}^b$, where $|\eta|$ is large, we can apply, for instance, the control law[1], $u_1 = k_s \mathrm{sgn}(s)$ and $u_2 = 0$ where k_s is some constant chosen by the user. A simple calculation shows that with this control law the system will leave $\mathcal{D}_{\bar{\eta}}^b$ in finite time. Moreover, it can be easily shown that for System I $\dot{\eta} = -(\mu/2 - k)\eta$ and, hence, the region $\mathcal{D}_{\bar{\eta}}^g := \Re^3 \backslash \mathcal{D}_{\bar{\eta}}^b$ is invariant. Thus, once the system enters $\mathcal{D}_{\bar{\eta}}^g$ it stays there for all future times. Once in $\mathcal{D}_{\bar{\eta}}^g$, the control law (5) can be used. During controller implementation, $\bar{\eta}$ was chosen by trial and error so as to achieve reasonable control input and state transient responses. For System II, it is shown in the Appendix that η remains bounded along closed-loop trajectories and the region $\mathcal{D}_{\infty}^g$ is positively invariant. This modification of Controller 1 was implemented in both Systems I and II.

B. Controller 2

The second time-invariant controller also uses ideas from invariant manifold theory. This controller, however, provides a control input which is explicitly bounded by an *a priori* specified upper bound, regardless of the initial conditions. This controller was originally developed for the stabilization problem of underactuated axisymmetric spacecraft in [19]. It is modified here for the case of a unicycle-type mobile robot.

The proposed control law is given by

$$\begin{aligned} u_1 &= -k\frac{x_1}{\sqrt{\nu^2 + 1}} + \mu\, \mathrm{sat}_2(s, \nu) \\ u_2 &= -k\frac{x_2}{\sqrt{\nu^2 + 1}} - \mu\, \mathrm{sat}_1(s, \nu) \end{aligned} \tag{8}$$

[1]Notice that the system (3a) or (4a) is controllable on the x_3 axis.

where $\nu = \sqrt{x_1^2 + x_2^2}$ and k and μ are constants satisfying

$$\mu > 2k > 0, \qquad \text{if } |\eta| < 1 \tag{9a}$$

$$\mu > -2k > 0, \qquad \text{if } |\eta| \geq 1. \tag{9b}$$

The saturation functions $\mathrm{sat}_i \ (i = 1, 2)$ are defined as

$$\mathrm{sat}_i(s, \nu) = \begin{cases} \mathrm{sat}\left(\frac{s}{\nu}\right)\frac{x_i}{\nu}, & \text{if } \nu \neq 0 \\ \mathrm{sgn}(s), & \text{if } \nu = 0 \end{cases} \tag{10}$$

where $\mathrm{sat}(x) := \min\{1, |x|\}\mathrm{sgn}(x)$.

Proposition 3: The control law given by (8)–(10) almost exponentially stabilizes System I. Moreover, the control input is bounded by $|u_{1,2}| \leq |k| + |\mu|$.

Proof: The proof is similar to the one in [19] and [2] and, thus, is omitted. ■

Remark 2: The value of unity in (9) is chosen for the sake of simplicity. Any other convenient bound can be selected according to the desired decomposition of the state space. Of course, the saturation function in (10) has to be modified accordingly in this case.

Although Controller 2 guarantees an *a priori* upper bound for u_1, u_2, and ω, it does not provide such a bound for v [see (3b)]. Using System II for implementation, we explicitly ensure that v and ω remain bounded.

Proposition 4: For $k > 0$ and $\mu > 0$, the control law in (8) and (10) asymptotically stabilizes System II for all initial conditions $x \in \Re^3$. Moreover, the control input is bounded by $|u_{1,2}| \leq |k| + |\mu|$.

Proof: See the Appendix. ■

It should be mentioned at this point that by defining instead

$$\mathrm{sat}_i(s, \nu) = \mathrm{sat}\left(\frac{x_i}{\nu^2}\right)\mathrm{sgn}(s), \qquad i = 1, 2 \tag{11}$$

in (10) one obtains the bounded controller derived in [2] for the nonholonomic Brockett integrator.

IV. Controllers Tested

In this section, we give six additional controllers that were implemented on the Khepera robot. Two of them are time invariant [8], [1] and the rest are time varying (periodic) [16], [10], [15], and [12]. Table I summarizes the controllers tested. The stability proofs of these controllers can be found in the relevant references.

V. Controller Implementation

A. Khepera Robot

The implementation of all controllers was done on a Khepera mobile robot. The Khepera robot, shown in Fig. 2, is a product of the K-Team (`http://www.k-team.com`). It is a mobile robot with two dc motor-driven wheels. The dc motors are connected to the wheels through a $25:1$ reduction gear box. Two incremental encoders are placed on the motor axes. The resolution of each encoder is 24 pulses per revolution of the motor axis. This corresponds to $24 \times 25 = 600$ pulses per revolution of the wheels or 12 pulses/mm of wheel displacement. The algorithm for estimating the velocity from the encoder outputs is implemented on the robot. For dc-motor speed control, a native

TABLE I
CONTROLLERS TESTED

Controller	Ref.	Comments
1	[17],[2]	Discontinuous, Exponential Convergence
2	[19],[2]	Discontinuous, Bounded, Exponential Convergence
3	[8]	Two-stage switching, Time-Invariant controller
4	[1]	Time-Invariant, Polar Coordinates
5	[16]	Time-Varying
6	[10]	Time-Varying
7	[15]	Time-Varying
8	[12]	Time-Varying, Exponential Convergence

PID controller is implemented on the Khepera robot. All one then needs to do in order to control Khepera is to read position signals and issue velocity commands via the RS-232 serial port. The maximum sampling rate can be up to 100 Hz owing to the limitation of the RS-232 serial communication (maximum is 4.8 kB/s for the Khepera robot). For all experiments in this paper, we used 50 Hz for sampling.

B. Implementation of Controllers on a Windows NT Environment

A specially written C++ application running under Windows NT was developed by the authors to control the robot via an RS-232 serial port. A Pentium II 400 MHz class PC running Windows NT 4.0 was used as the host computer. The velocity commands were sent to the robot through the RS-232 serial port. Position information was obtained through the encoders. Since WinNT is not a real-time operating system, a timer handler was called periodically to implement the control laws. The 32-bit multimedia timer service for the Windows NT application level was used. With this timer service, a resolution of up to 1 ms can be achieved.

C/C++ was used to implement the control algorithms with a nice looking, multitabbed dialog box interface, shown in Fig. 3. Several tabs can be used to set up the stabilization or tracking problems, change controller gains, sampling frequency, configure the dc motors, etc. To record the history of the control input and robot response without recording time limitations, a double-buffered data storage algorithm was developed. The robot motion can also be visualized by an independent OpenGL Window that supports 6-DOF camera navigation using the keyboard (not shown in Fig. 3). The software is available from the authors upon request.

C. Position Estimation

Since there is no direct measurement of the absolute position and orientation of the robot, we need to estimate the position of the robot from wheel displacement information. This common procedure, called *dead reckoning*, uses geometric relations of the wheel displacements and the robot position to estimate the position of the robot.

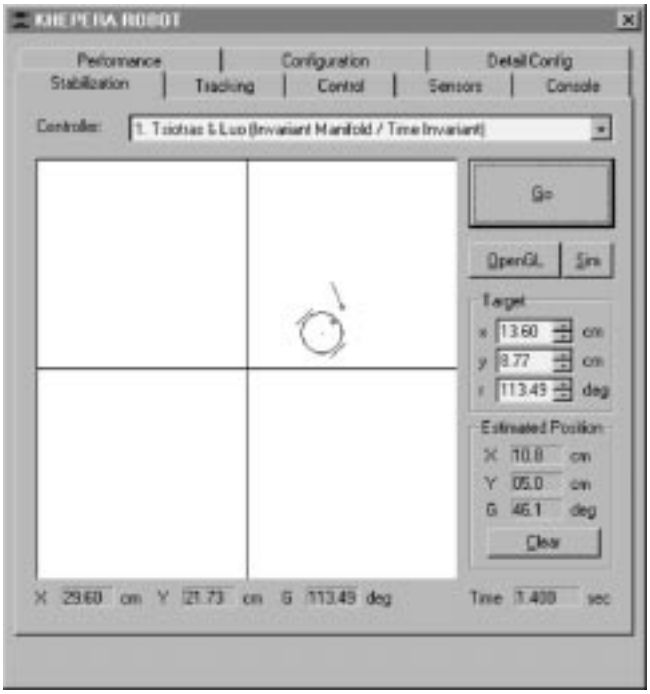

Fig. 3. Robot control program panel.

The position estimation error was checked by a series of experiments. Before each experiment, the robot was placed at a point (x_0, y_0) with heading angle γ_0 and was commanded to go to the origin. At the end of each experiment, the actual position of the robot (measured on a 1 mm-resolution grid) was compared with the estimated position and orientation using the dead-reckoning scheme and the error was recorded. The mean estimation error (x_e, y_e, γ_e) was deduced from a sequence of five experiments for each set of initial conditions. The accuracy of the dead-reckoning scheme was deemed to be adequate for the objectives of our experiments.

D. Motor and Robot Dynamics

A common tacit assumption made for all controllers tested is that the system has ideal response, i.e., there are no dynamics. This is not true for the Khepera robot, which uses dc motors. dc motors usually have poor transient response when compared, for example, with step motors. Moreover, the left and right motors may not have identical responses owing to nonhomogeneous mass distribution over the robot body or differences in the motors themselves. We therefore used the following procedure to characterize the dynamic behavior of the motors.

With the robot initially at rest, a right ($v_1 = 423$ mm/s, $v_2 = 377$ mm/s) and a left ($v_1 = 377$ mm/s, $v_2 = 423$ mm/s) turn were commanded, and the robot wheel velocities were recorded. These are shown in Fig. 4. From this figure, it is seen that the linear velocity v has a typical step response, but the angular velocity ω has an unusual response. During the right turn, small velocity differences in v_1 and v_2 are evident. As a result, the

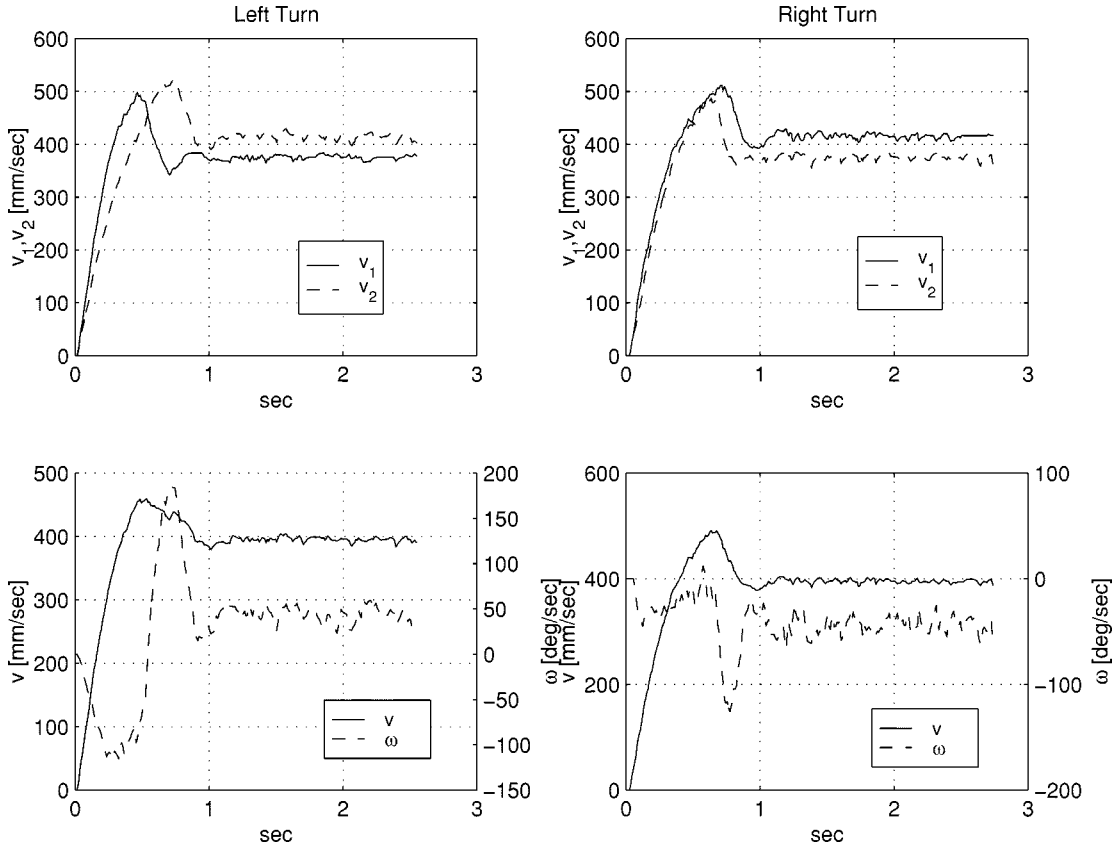

Fig. 4. Step responses of linear and angular velocities.

angular velocity is relatively small for about 0.6 s. This can be treated as a delay. Moreover, comparing the response of the left wheel v_1 in a left and a right turn, one sees that the maximum overshoot time becomes smaller as the step input becomes smaller. This implies nonlinearity in the motor dynamics of the left wheel. Most importantly, because of this asymmetric response of the wheels, the angular velocity is initially reversed in a left turn. In fact, during the left turn, a negative angular velocity is produced for about 0.5 s. In summary, the difficulties caused by the motor dynamics are as follows: 1) there is relatively high overshoot, moreover, the maximum overshoot time depends on the magnitude of the applied step, hence some nonlinearities exist in the motor and 2) the left and right motor seem to have different dynamics. As a result, the linear and angular velocity responses are coupled.

Based on the motor velocity step responses, a parameter identification scheme was used to fit a second-order transfer function that approximates the motor dynamics from commanded to output velocity. This dynamic model was used to validate the often unusual behavior observed for some controllers when implemented on the real system.

E. Velocity Output Quantization

The velocity command of the Khepera robot is quantized by 8 mm/s. This is not important if the velocity is large. However, as the states converge to the origin, quantization becomes more important because the velocity command is small around the origin. At the origin, quantization manifests itself as a dead-zone problem, resulting in a steady-state error. This steady-state error in γ was more severe for Controllers 1 and 4 (about 15°–60°). One simple, but effective, approach to handling this problem is to use an inverted dead zone. That is, the magnitude of the velocity commands was increased by the amount of quantization. The improvement in the steady-state error (especially for the heading angle γ) using the inverted dead zone is shown in Fig. 5. The inverted dead zone was implemented in software.

F. Scaling

A nonlinear system has different characteristics, depending on the region where it operates in the state space. For certain regions, it may exhibit small oscillations, fast convergence rates, and good robustness, while for other regions it may exhibit large oscillations and slow convergence rates. Since the performance for nonlinear systems is not uniform, it is of interest to properly scale the differential equations to account for this behavior. Scaling is equivalent to choosing appropriate units for the system variables or proper controller gains. By proper scaling, one can avoid the regions of poor performance. This helps to design better controllers. The importance of scaling in improving transient response has also been noted by other authors [11]. Fig. 6 shows how scaling was applied to the Khepera robot.

G. Effect of Sensor Noise and Quantization

Typically, sensor noise and quantization result in a limit cycle. Some controllers were much more sensitive to sensor noise than

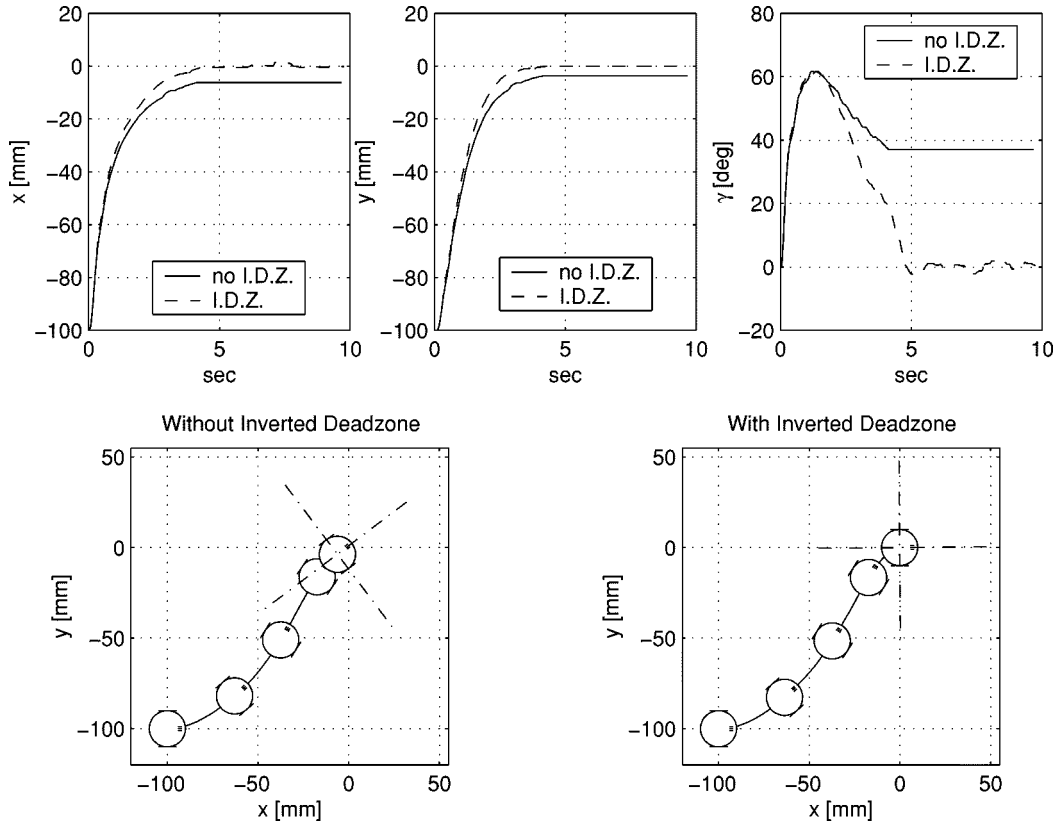

Fig. 5. Improvement of steady-state error using inverted dead zone for Controller 1 and System II.

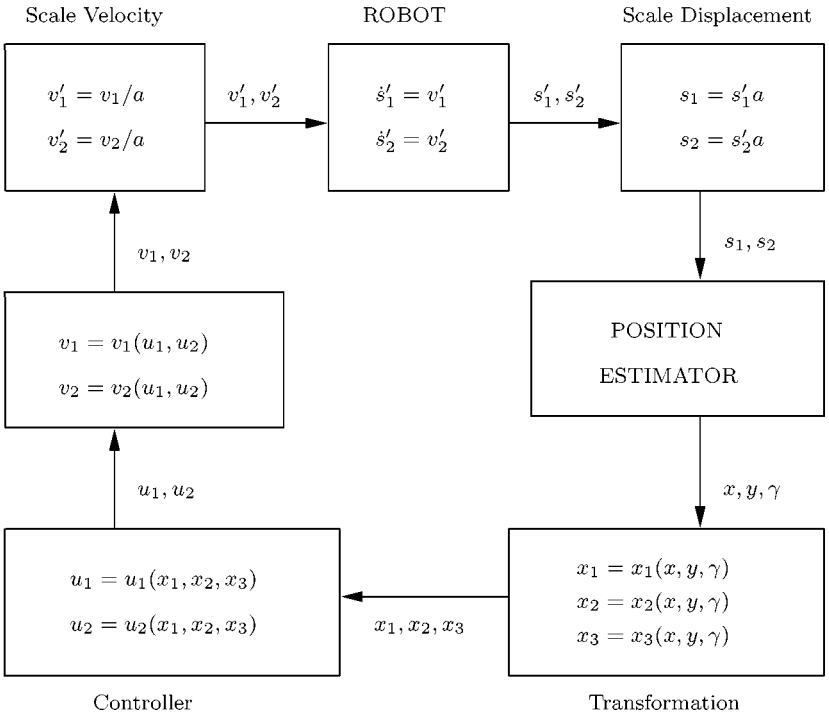

Fig. 6. Block diagram of robot control system including scaling.

others. Fig. 7 shows the effects of sensor noise for Controllers 2 and 4. As shown in this figure, Controller 4 is especially sensitive to noise. The sensitivity of Controller 4 to sensor noise is elaborated upon later.

VI. Experimental Results

To compare the controllers, we introduced four different missions. Due to the nonholonomic constraint, missions where the

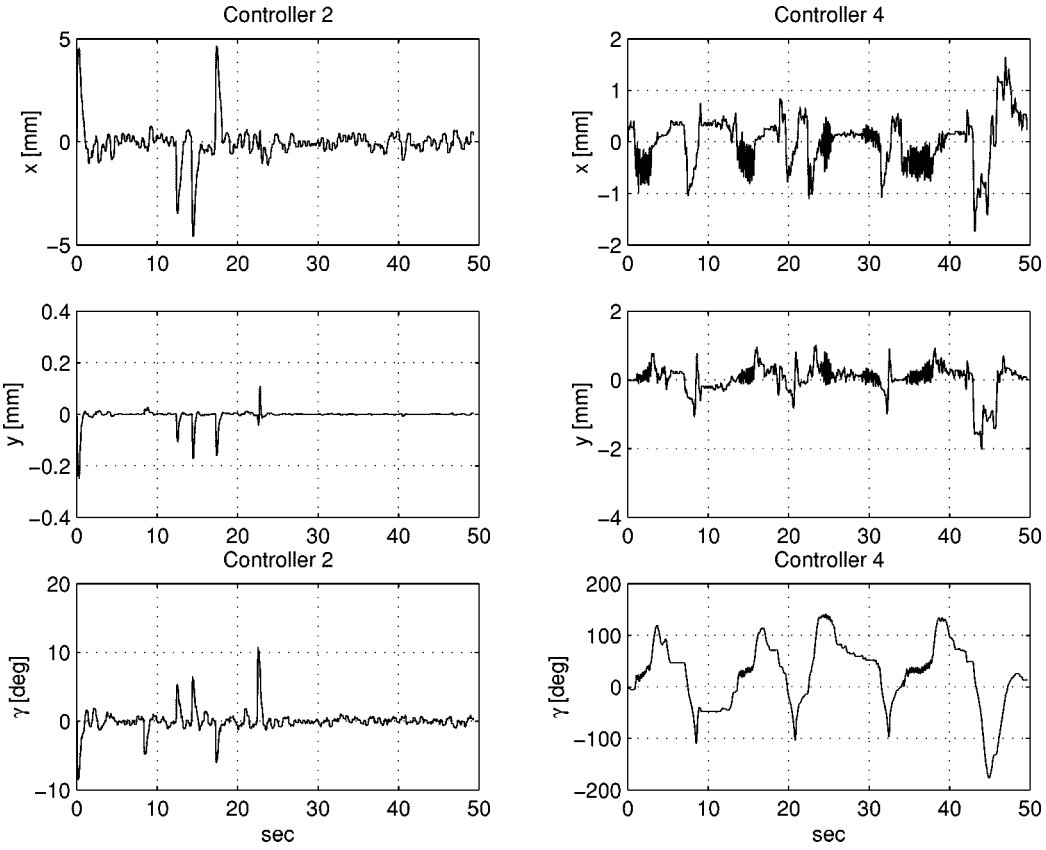

Fig. 7. Effects of noise on steady-state error.

TABLE II
INITIAL CONDITIONS FOR ROBOT MISSIONS

Mission	x (mm)	y (mm)
Easy	-100	-25
Normal	-100	-100
Singular (Parallel Parking)	0	-100
Long Distance	-500	-500

robot is commanded to move sideways (i.e., in violation of this constraint) were assumed to be more challenging. We therefore designed four missions: 1) easy mission: the forward distance to be travelled is larger than the sideways distance; 2) normal mission: the forward and sideways distances are the same; 3) singular mission: the robot is commanded to move sideways (this mission is customarily referred to as the "parallel parking maneuver"); and 4) long-distance mission: the robot is commanded to travel over a large distance. Depending on the aggressiveness of the controller (most time-invariant controllers can be classified as such) the motors may saturate during a long-distance mission. Moreover, this mission can be used to estimate the region of attraction for some controllers that only ensure local asymptotic stability.

The initial conditions for all missions are given in Table II. For all missions, the initial heading angle γ is chosen to be zero. Starting from these initial conditions, and for all cases, the robot was commanded to go to the origin.

A. Discussion of Results

Controllers 1 and 2: Figs. 8 and 9 show the plots of selected trajectories for Controllers 1 and 2. As shown in these figures, Controllers 1 and 2 may fail to achieve convergence for System I for some cases. Subsequent analysis showed that the divergence was due to motor dynamics. Numerical simulations including a motor model (see Section V-D) validated the results of Figs. 8 and 9. For System II, however, both controllers achieved stability for all missions. Fig. 10 shows a comparison between the actual and commanded velocities for Controllers 1 and 2 when applied to System II. Controller 2 (which guarantees bounded input commands) behaves as expected, whereas Controller 1 exhibits large magnitude for v.

Controller 3: Similarly to Controller 1, this controller needs to be modified inside the region $\mathcal{D}_{\bar{\eta}}^{\rho}$ to avoid the singularity when $x_1 = x_2 = 0$. The approach of Section III was used to circumvent the singularity issue. Nonetheless, this controller induces chattering, as can be verified from the top left plot of Fig. 11. This figure shows the results for a normal mission using System I and with gains $k = 1$, $\mu = 3$, and scaling $= 100$.

Controller 4: This controller does not use either System I or System II. Instead, its derivation and implementation uses polar coordinates [1]. The experimental results for Controller 4 are shown in Fig. 12. This controller has good convergence and good transient response for all cases. Fig. 12 shows the results for a singular mission with gains $k_1 = 1$, $k_2 = 1$, $k_3 = 1$,

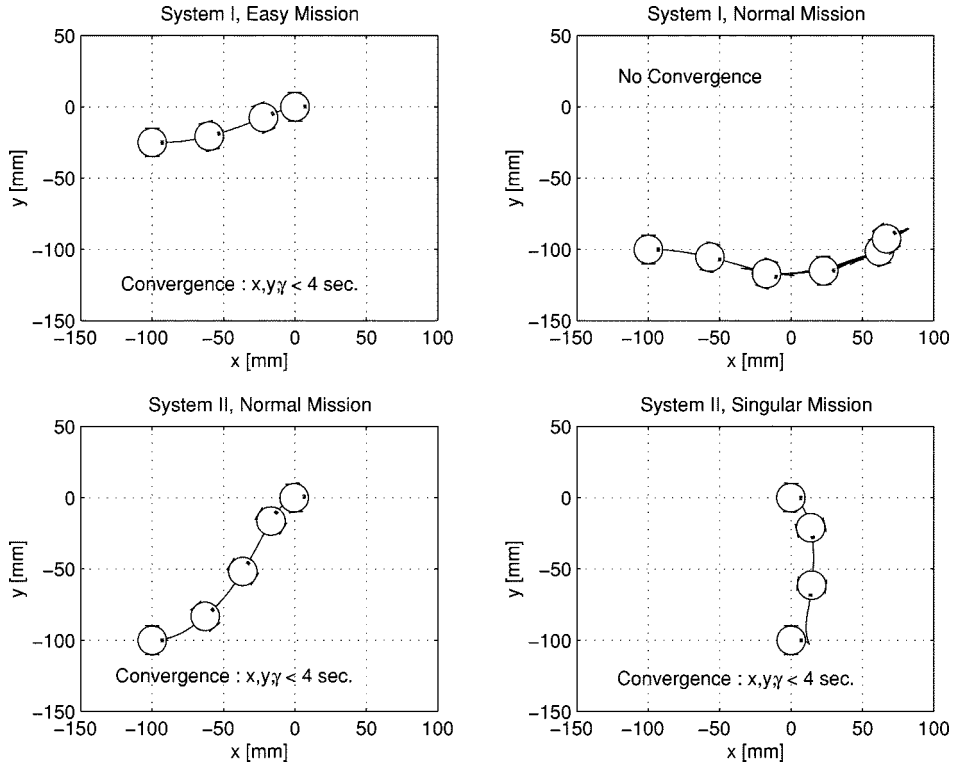

Fig. 8. Selected trajectories for Controller 1.

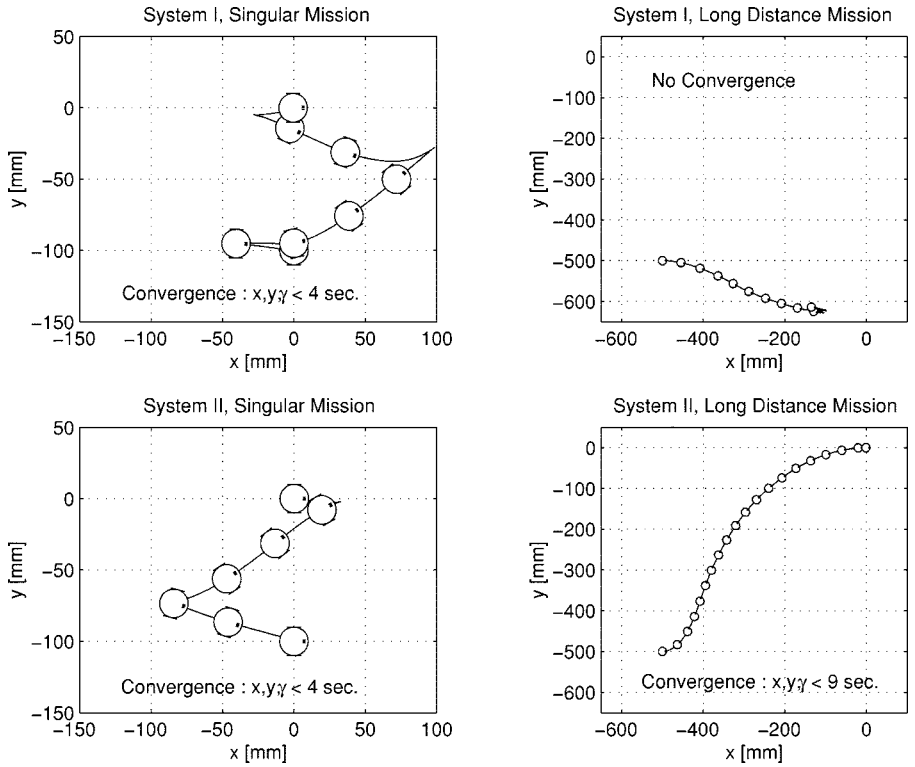

Fig. 9. Selected trajectories for Controller 2.

and scaling $= 1$. A potential problem with this controller is a steady-state error for the heading angle γ, due to the dead zone in the velocity output (see upper right and lower left plots of Fig. 12). Our simulations, with different levels of sensor noise, indicated that Controller 4 was sensitive to sensor noise, resulting in a limit cycle for the heading angle around the origin. These simulations were verified by the experiments. Controller 4 basically implements a "turn–drive–turn" strategy. Although this control strategy is intuitive and simple to implement, it may lead to large angular velocity commands close to the origin. This

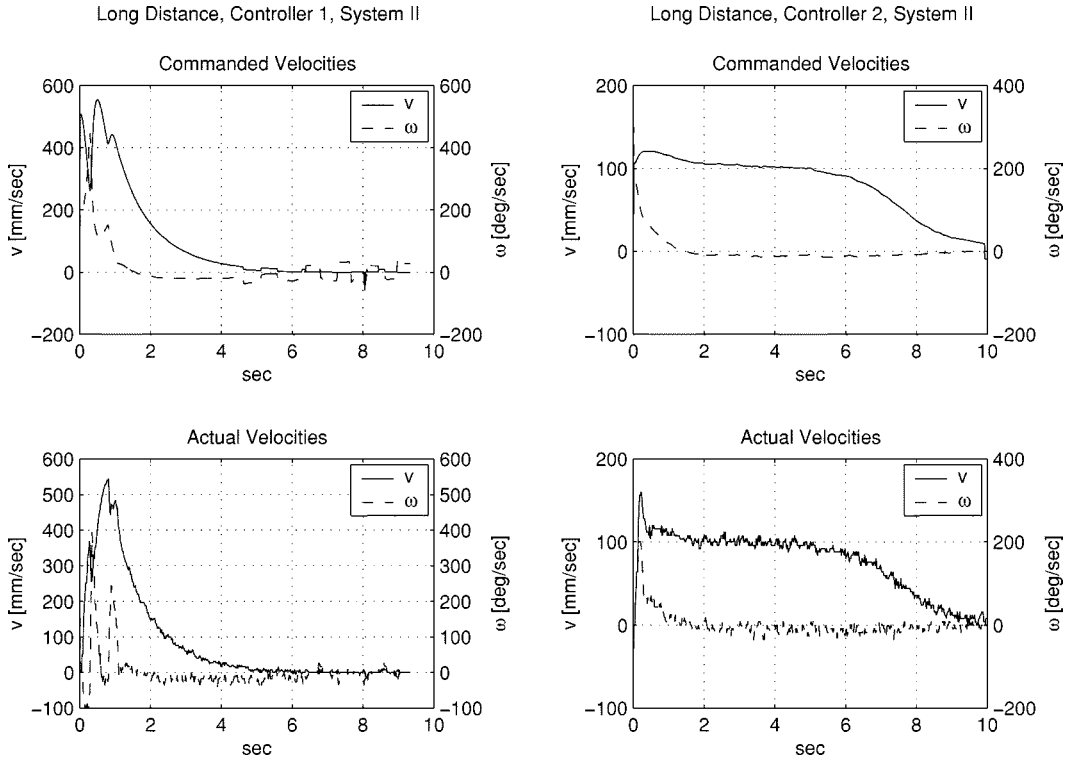

Fig. 10. Commanded and actual velocity comparison for Controllers 1 and 2 applied to System II.

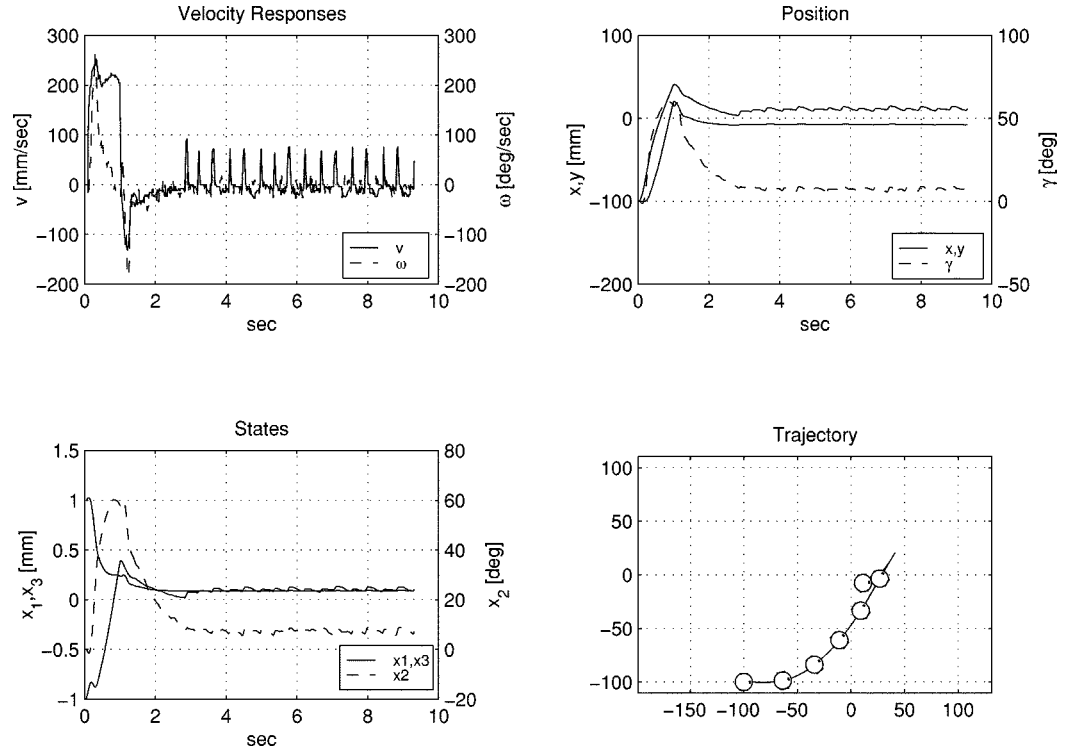

Fig. 11. Experimental results for Controller 3.

is because the angular velocity command ω for this controller does not depend on the distance from the origin [1]. Therefore, even small errors in x and y coordinates may produce large angular velocity commands and, hence, steering angles. Since this controller is inherently sensitive to noise and small perturbations around the origin, we cannot apply the inverted dead zone to reduce this steady-state error. The sensitivity of this controller to noise close to the origin has also been observed in [3]. Overall, this controller can have a very good performance if a method to avoid the heading oscillations is devised.

Controllers 5, 6, and 7: Controller 5 from [16] exhibited very slow converge when implemented in both Systems I and

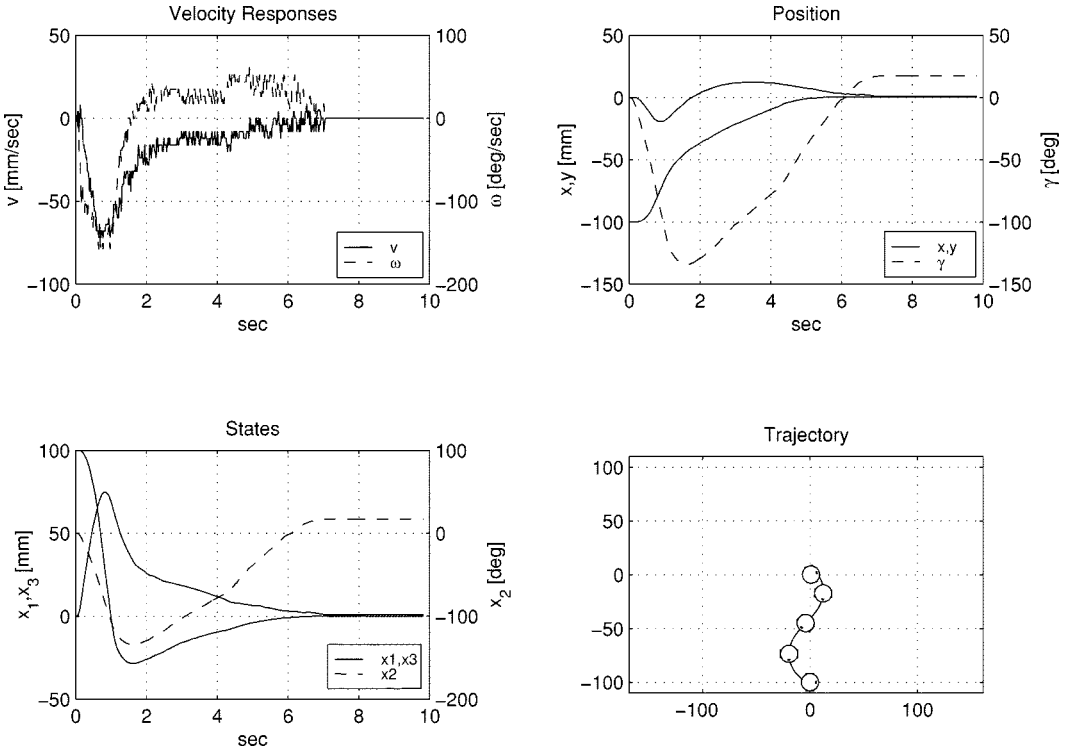

Fig. 12. Experimental results for Controller 4.

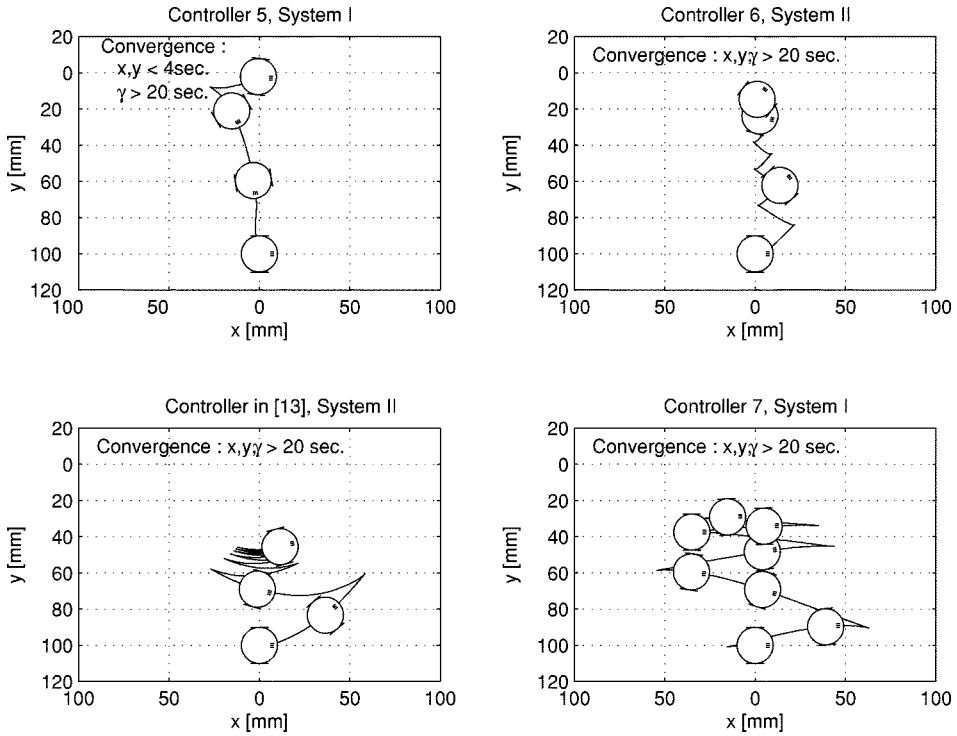

Fig. 13. Trajectories of Controllers 5, 6, and 7 for the singular mission. The controller from [13] is also shown for comparison.

II. Controller 6 has been derived in [10] using System I. In this paper, we used System II for the implementation since it leads to better convergence. The advantages of using System II instead of System I have also been observed by M'Closkey and Murray [11], where the authors used center manifold theory to prove local asymptotic stability for System II. It should be pointed out that the controller of [11] was also implemented. The results of these experiments were similar to the ones for Controller 6 and are omitted. Controller 7 was implemented using System I. Implementation on System II gave similar results.

Fig. 13 shows that the time-varying Controllers 5, 6, and 7 have very slow or oscillatory behavior. Their performance can be improved by scaling the states or by choosing different gains, but this has only a limited effect. The slow convergence of the

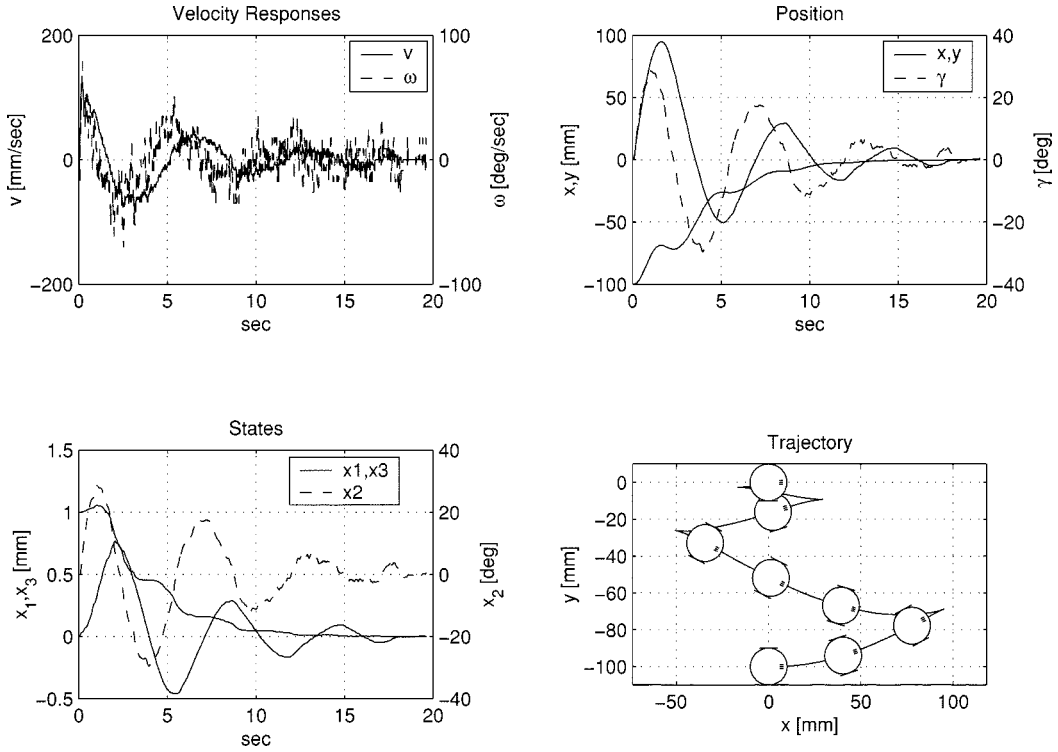

Fig. 14. Robot trajectories with Controller 8 and System II (singular mission).

time-varying controllers can be shown rigorously [9]. In all experiments and simulations in this paper, these controllers have shown poor performance.

Controller 8: The convergence rates of the time-varying controllers can be improved significantly using the scaling approach of [12]. In simulations, this controller achieved stability for both Systems I and II. The speed of converge was about 15–25 s, regardless of the magnitude of the initial conditions. However, in experiments, it failed to converge when the initial conditions were larger than about 50 mm using System I (for singular and normal missions). For the easy mission, the robot converged for all initial conditions. Applying proper scaling and/or choosing System II for implementation solved this problem. Then the robot converged with good transient response. Nonetheless, its convergence was still slower than the time-invariant controllers. Results of the experiments with this controller for the singular mission are shown in Fig. 14.

B. Summary

Table III summarizes the results of the experiments. In Table III the letters "E", "N", "S" and "L" stand for easy, normal, singular, and long-distance missions respectively. "E" stands for "excellent," which means good speed of response, no oscillations either in x, y, or γ, reasonable control inputs and natural trajectories. "G" stands for "good," which means that the convergence is acceptable, i.e., within 10 s. "S" stands for "slow," which means that it took the robot more than 20 seconds to converge. "C" stands for "chattering," which means that trajectories converged, but there was too much chattering in the velocity commands. "O" stands for "oscillatory," which means that the trajectory oscillated around the origin. "U" stands for "unstable/unsatisfactory" response.

TABLE III
SUMMARY OF EXPERIMENTAL RESULTS

Ctr.	Sys.	E	N	S	L	Note
1	I	E	O	O	O	Oscillatory
	II	E	E	E	E	Good/Fast
2	I	E	O	O	O	Oscillatory
	II	E	E	E	E	Good/Fast/Bounded
3	I	C	C	C	O	Chattering
	II	C	C	C	C	
4	Polar	E in x, y, O in γ				Good/Fast/Noise
5	I/II	G	S	S	O	Very Slow
6	I	U	U	U	U	Diverged
	II	S	S	S	S	Very Slow
7	I/II	S	S	S	O	Very Slow
8	I/II	G	G	G	G	Good/Slow

As indicated by the table, Controller 2 (when implemented on System II) gave the most satisfactory performance for all missions. Its speed of response and the velocity commands were always within acceptable limits. The implementation complexity of all controllers was comparable, with the discontinuous Controllers 1 and 3 requiring the most care to avoid singularities. Controller 2 has a built-in mechanism that avoids singular regions. Controllers 2 and 4 generated natural trajectories, i.e., similar to what a human operator would attempt. However, as mentioned previously, Controller 4 was sensitive to sensor noise, resulting in relatively large limit cycles of the heading angle around the origin. Time-varying controllers generated oscillatory paths, and all of them showed slow convergence, especially close to the origin. Among

the time-varying controllers, Controller 8 exhibited the best performance and speed of response. The implementation of this controller presented the most difficulties, however, because of the requirement to update the parameter λ of the dilation operator (see [12]) using a Newton method at each time step.

VII. Conclusions

In this paper, we have experimentally tested several stabilizing controllers for a unicycle-type mobile robot. In theory, all controllers ensure (at least) some form of local asymptotic stability/convergence. In our experiments, several of these controllers exhibited oscillatory or even unstable behavior. Several issues contributed to this, including motor dynamics, sensor and quantization errors, actuator dead zone, etc. By applying several techniques (such as inverse dead zone, scaling, etc.), the performance of most controllers improved significantly. All time-varying controllers except the controller in [12] were too slow and oscillatory for most practical purposes. In fact, this controller was the only time-varying controller with acceptable performance and speed of response. The two time-invariant controllers presented in this paper showed consistently good performance for all missions, if implemented properly. Of course, more experiments are required to confirm these conclusions.

Appendix

In this section, we make use of the theory of homogeneous systems and dilation operators; see, for example, [12] for a detailed discussion on the subject. For our purposes, it suffices to say that for any set of positive scalars $r_i > 0$, $i = 0, \ldots, n$, the dilation operator Δ_λ^r is defined as $\Delta_\lambda^r x = [\lambda^{r_1} x_1 \quad \lambda^{r_2} x_2 \quad \ldots \quad \lambda^{r_n} x_n]^T$, $\lambda > 0$. The homogeneous norm associated with the dilation Δ_λ^r is a continuous function $\rho: \Re^n \to \Re_+$, such that 1) $\rho(x) \geq 0$, and $\rho(x) = 0$ if and only if $x = 0$; and 2) $\rho(\Delta_\lambda^r x) = \lambda \rho(x)$. Such a norm always exists. A vector field $f: \Re^n \to \Re$ is homogeneous of degree k with respect to the dilation Δ_λ^r if $f(\Delta_\lambda^r x) = \lambda^k f(x)$.

We are now ready to provide the proof of Proposition 2.

A. Proof: Proposition 2

Let $f(x) = [u_1(x), \ u_2(x), \ x_1 u_2(x)]^T$ and $g(x) = [-x_3 u_2(x), \ 0, \ 0]^T$, where $u_1(x)$ and $u_2(x)$ as in (5). Then the equation for System I is given by $\dot{x} = f(x)$, and the equation for System II is given by $\dot{x} = f(x) + g(x)$. Let $U(x) = (1/2)\left(x_1^2 + x_2^2 + x_3^2\right)$. The derivative of U along the trajectories of System II is given by $\dot{U} = -k\left(x_1^2 + x_2^2\right) \leq 0$ for all $x \in \mathcal{D}_\infty^g := \Re^3 \backslash \mathcal{D}_\infty^b$. It follows that the closed-loop trajectories are bounded inside $\mathcal{D}_\infty^g$.

Let now $\zeta = 1/\left(x_1^2 + x_2^2\right)$. Along the closed-loop trajectories of System II with Controller 1, one can verify that

$$\dot{\zeta} = 2k\zeta - 2k\left(\frac{x_1 x_2}{x_1^2 + x_2^2}\right) x_3 \zeta - 2\mu\left(\frac{x_1^2}{x_1^2 + x_2^2}\right) x_3 s \zeta^2. \quad \text{(A1)}$$

Notice that the terms in parentheses are bounded in any neighborhood of the origin. From the inequality $s^2 - |s|/4\zeta \leq x_3 s \leq s^2 + |s|/4\zeta$, it follows that the coefficient of ζ^2 in (A1) is nonpositive for large ζ. Hence, $\dot{\zeta} \leq 0$ for large ζ, and since $\zeta > 0$ it follows that (A1) cannot have finite escape times. Equivalently, $x_1^2 + x_2^2$ cannot become zero in finite time. It follows that the set $\mathcal{D}_\infty^g$ is positively invariant for System II with Controller 1.

In order to show convergence, let $V(x_1, x_2, x_3) = (1/2)\left(x_1^2 + x_2^2\right)^2 + s^2$. The derivative of V along System I is given by[2]

$$\dot{V} = L_f V(x) = -2k\left(x_1^2 + x_2^2\right)^2 - \mu s^2 \leq -\gamma V(x) < 0 \qquad \forall\, x \in \mathcal{D}_\infty^g$$

where $\gamma = \min\{4k, \mu\} > 0$. This shows that System I with Controller 1 is almost exponentially stable with respect to the set $\mathcal{D}_\infty^g$ (recall that the set $\mathcal{D}_\infty^g$ is positively invariant for System I with Controller 1 [17]).

The derivative of V along the closed-loop trajectories of System II is given by $\dot{V} = L_f V(x) + L_g V(x)$, where

$$L_g V(x) = -2\left(x_1^2 + x_2^2\right) x_1 x_3 u_2(x) + s x_2 x_3 u_2(x).$$

A straightforward calculation shows that $L_g V(x)$ is bounded in every neighborhood of the origin.

Consider now the dilation $\Delta_\lambda^r x = [\lambda x_1, \ \lambda x_2, \ \lambda^2 x_3]^T$. Using this dilation, one can verify that $u_1\left(\Delta_\lambda^r x\right) = \lambda u_1(x)$ and $u_2\left(\Delta_\lambda^r x\right) = \lambda u_2(x)$. Thus, the control law in (5) is homogeneous to degree one with respect to the dilation $\Delta_\lambda^r x$. Moreover, since $L_f V(\Delta_\lambda^r x) = \lambda^4 L_f V(x)$ and $L_g V\left(\Delta_\lambda^r x\right) = \lambda^6 L_g V(x)$, then $L_f V$ and $L_g V$ are homogeneous functions of degrees four and six, respectively.

Consider now the homogeneous norm $\rho(x)$ associated with the given dilation Δ_λ^r.[3] We claim that there exists $c > 0$ such that for all $0 < \rho(x) \leq c$, $|L_f V(x)| > |L_g V(x)|$. To prove this result, we first show that

$$\min_{\rho(x)=c} \sqrt{\frac{|L_f V(x)|}{|L_g V(x)|}} > 1$$

implies

$$\min_{\rho(x)\leq c} \sqrt{\frac{|L_f V(x)|}{|L_g V(x)|}} > 1.$$

To this end, let any x such that $\rho(x) = c$, and consider the set of points $y = \Delta_\lambda^r x$ for $0 < \lambda \leq 1$. Notice that $\rho(y) = \rho(\Delta_\lambda^r x) = \lambda \rho(x) \leq c$. Conversely, for every y with $\rho(y) \leq c$, there exists $0 < \lambda \leq 1$ such that $y = \Delta_\lambda^r x$ with $\rho(x) = c$. From the homogeneous properties of $L_f V$ and $L_g V$, it now follows that

$$\sqrt{\frac{|L_f V(y)|}{|L_g V(y)|}} = \sqrt{\frac{|L_f V(\Delta_\lambda^r x)|}{|L_g V(\Delta_\lambda^r x)|}} = \frac{1}{\lambda}\sqrt{\frac{|L_f V(x)|}{|L_g V(x)|}} > \frac{1}{\lambda} \min_{\rho(x)=c} \sqrt{\frac{|L_f V(x)|}{|L_g V(x)|}} > \frac{1}{\lambda} \geq 1.$$

To complete the proof of our claim, let

$$\lambda^* = \min_{\rho(x)=1} \sqrt{\frac{|L_f V(x)|}{|L_g V(x)|}}. \quad \text{(A2)}$$

[2]As usual, $L_f V$ denotes the Lie derivative of the function V along the vector field f.

[3]Choose, for instance, $\rho(x) = (x_1^4 + x_2^4 + x_3^2)^{1/4}$.

Since $L_fV(x)=0$ if and only if $x=0$ and $L_gV(x)$ is bounded on every neighborhood of the origin, it follows that $\lambda^*>0$. If $\lambda^*>1$, let $c=1$ and the result follows. Otherwise, let a positive scalar c such that $c<\lambda^*\leq 1$ and consider the set $p(x)\leq c$. Noticing that $\{x:\rho(x)=c\}=\{\Delta_c^r y:\rho(y)=1\}$, one obtains that for any x such that $\rho(x)=c$, the following holds:

$$\min_{\rho(x)=c}\sqrt{\frac{|L_fV(x)|}{|L_gV(x)|}}=\min_{\rho(y)=1}\frac{1}{c}\sqrt{\frac{|L_fV(y)|}{|L_gV(y)|}}=\frac{\lambda^*}{c}>1.$$

Hence

$$\min_{\rho(x)\leq c}\sqrt{\frac{|L_fV(x)|}{|L_gV(x)|}}>1.$$

Therefore, there always exists a neighborhood of the origin such that $|L_fV(x)|>|L_gV(x)|$. Since $L_fV(x)<0$, this implies that there exists $\epsilon>0$ such that $\dot V=L_fV(x)+L_gV(x)<0$ for all $x\in(\Re^3\backslash\mathcal{D}_\infty^b)\cap\mathcal{B}_\epsilon$. This implies local almost asymptotic stability about the origin. Consequently, $\lim_{t\to\infty}(x_1(t),x_2(t),x_3(t))=0$.

In order to show that the control inputs remain bounded for $\mu>2k>0$, it suffices to show that η in (7) remains bounded along closed-loop trajectories. From the previous analysis, it follows that η cannot go to infinite in finite time. We next show that η remains bounded for all $t\geq 0$. First, notice that

$$\begin{aligned}\lim_{t\to\infty}|x_1(t)||\eta(t)|&=\lim_{t\to\infty}\frac{|x_1(t)|}{\sqrt{x_1^2(t)+x_2^2(t)}}|s(t)|\\&\leq\lim_{t\to\infty}|s(t)|=0.\end{aligned}$$

Hence, $|x_1||\eta|\to 0$ as $t\to\infty$. Therefore, for every $\epsilon>0$ there exists $T>0$, such that $|x_1(t)||\eta(t)|<\epsilon/(k+\mu)$ for all $t\geq T$. A simple calculation shows that

$$\begin{aligned}\frac{1}{2}\frac{d\eta^2}{dt}=&-\left(\frac{\mu}{2}-k\right)\eta^2-\frac{k}{2}x_2^2\eta^2-\left(\frac{\mu}{4}+\frac{k}{2}\right)\theta^2\eta^2\\&-\frac{\mu}{2}\theta\left(1+\frac{x_1^2}{\nu^2}\right)\eta^3-k\theta\eta^3-\frac{k}{4}\theta x_2^2\eta-\mu\frac{x_1^2}{\nu^2}\eta^4\end{aligned}$$

where $\theta=x_1x_2/\sqrt{x_1^2+x_2^2}$ and $\nu=\sqrt{x_1^2+x_2^2}$. From the inequalities $|\theta|\leq|x_i|$, $(i=1,2)$, and $x_1^2/\nu^2\leq 1$, it follows that

$$\frac{1}{2}\frac{d\eta^2}{dt}\leq-\alpha\eta^2+\pi|x_1||\eta|^3+\frac{k}{4}|\theta|x_2^2|\eta|-\mu\frac{x_1^2}{\nu^2}\eta^4\qquad\text{(A3)}$$

where $\alpha:=\mu/2-k>0$ and $\pi:=\mu+k$. Since x_1 and x_2 are bounded, there exists $c_i>0$ such that $|x_i(t)|<c_i$ for all $t\geq 0$, where $i=1,2$. Consequently

$$\begin{aligned}\frac{1}{2}\frac{d\eta^2}{dt}\leq&-\alpha\eta^2+\epsilon\eta^2+\frac{k}{4}c_2^3|\eta|-\mu\frac{x_1^2}{\nu^2}\eta^4\\\leq&-(\alpha-\epsilon)|\eta|\left(|\eta|-\frac{kc_2^3}{4(\alpha-\epsilon)}\right)\ \forall\, t\geq T.\end{aligned}\qquad\text{(A4)}$$

Therefore, if for any time $t\geq T$, $|\eta|$ becomes larger than $kc_2^3/4(\alpha-\epsilon)$, the derivative of η is negative semidefinite. Since ϵ is arbitrary, it follows that η is bounded along the closed-loop trajectories if $\mu>2k>0$. ■

B. Proof: Proposition 4

First, the fact that the control inputs are bounded by $|k|+\mu$ follows directly from (8).

Next, consider the radially unbounded, positive-definite function $V=x_1^2+x_2^2+x_3^2$. Its derivative along (4a) with control law (8) is calculated as

$$\begin{aligned}\dot V=&2x_1\left(-k\frac{x_1}{\sqrt{\nu^2+1}}+\mu\,\mathrm{sat}_2(s,\nu)\right)\\&+2x_2\left(-k\frac{x_2}{\sqrt{\nu^2+1}}-\mu\,\mathrm{sat}_1(s,\nu)\right)\\=&-2k\frac{x_1^2+x_2^2}{\sqrt{x_1^2+x_2^2+1}}\leq 0.\end{aligned}\qquad\text{(A5)}$$

The previous equation holds, regardless of whether $|\eta|<1$ or $|\eta|\geq 1$. In particular, $\dot V=0$ if and only if $x\in\mathcal{D}_\infty^b\cup\{0\}$. Global stability follows.

Inequality (A5) implies that x_1, x_2, and x_3 remain bounded. Since u_1 and u_2 are bounded, $\dot x_1$ and $\dot x_2$ are also bounded. Thus, x_1 and x_2 are uniformly continuous. $\dot V$ is also uniformly continuous. Moreover, the limit of V exists since V is bounded from below and nonincreasing. From Barbalat's Lemma [7], it follows that $\lim_{t\to\infty}\dot V(t)=0$. We conclude that x_1 and x_2 go to zero.

From (A5), we have that x_1 and x_2 go to zero, and x_3 remains bounded. Since V has a limit, it follows that $\lim_{t\to\infty}x_3(t)=\bar x_3\in\Re$. Suppose that $x_1(t)\equiv 0$ for all $t\geq T$. Then $\dot x_1(t)=0$ and $\dot x_3(t)=0$ for all $t\geq T$ as well. Let us assume that $x_3(t)=\bar x_3\neq 0$ for all $t\geq T$. Notice that in this case, x_2 cannot become identically zero for $t\geq T$, since from $\dot x_2=u_2=0$ it follows that $\mathrm{sgn}(\bar x_3)=0$, a contradiction. From the definition of $\dot x_1$, and substituting $x_1=0$ and $x_3=\bar x_3$ in (8), it follows that

$$\min\left\{1,\left|\frac{\bar x_3}{x_2}\right|\right\}=-\frac{k}{\sqrt{x_2^2+1}}|\bar x_3||x_2|\quad\forall\, t\geq T$$

which is a contradiction. Hence, if $\bar x_3\neq 0$, x_1 cannot converge to zero in finite time. Continuing this reasoning, if $\bar x_3\neq 0$, and since $x_1\to 0$ and $x_2\to 0$, the following expressions hold inside $\mathcal{D}_\infty^g$

$$\begin{aligned}\dot x_1=&\mu\,\mathrm{sgn}(x_3)\frac{x_2}{\nu}+\mu\,\mathrm{sgn}(x_3)\frac{x_1}{\nu}x_3+\mathcal{O}(|\nu|)\\\dot x_2=&-\mu\,\mathrm{sgn}(x_3)\frac{x_1}{\nu}+\mathcal{O}(|\nu|)\end{aligned}\qquad\text{(A6)}$$

where $\mathcal{O}(|x|^p)$ denotes a term of order p, i.e., $f(x)=\mathcal{O}(|x|^p)$ if $\lim_{|x|\to 0}f(x)/|x|^p=c\in\Re$ and where we have used the fact that $\mathrm{sgn}(s)=\mathrm{sgn}(x_3)$ for x_1, x_2 sufficiently small (but nonzero). Using the previous expressions one obtains that

$$\dot\nu=\frac{x_1^2}{\nu^2}\,\mu\,|x_3|+\mathcal{O}(|\nu|)\qquad\text{(A7)}$$

where the first term in the previous expression is of order $\mathcal{O}(1)$. Hence, there exists a time T such that $\dot\nu\geq 0$ for all $t\geq T$. In other words, if $\bar x_3\neq 0$, there exists a neighborhood of the origin in the x_1-x_2 space such that $\nu=\sqrt{x_1^2+x_2^2}$ is nondecreasing for all $t\geq T$. This contradicts the fact that $\nu\to 0$ as $t\to\infty$. Hence, necessarily $\bar x_3=0$.

(A7) also shows that there exists a neighborhood of the s axis (i.e., $|\eta| \gg 1$), such that the vector field of the closed-loop system points away from this axis. In addition, if $x \in \mathcal{D}^b_\infty$ (i.e., $\nu = 0$ and $s \neq 0$), the control law (8) reduces to $u_1 = \mu\,\mathrm{sgn}(s)$ and $u_2 = -\mu\,\mathrm{sgn}(s)$ with $\mu > 0$. Since $s \neq 0$, it follows that if $x(t) \in \mathcal{D}^b_\infty$ for some $t \geq 0$, $x(t+) \notin \mathcal{D}^b_\infty$ and x leaves $\mathcal{D}^b_\infty$. In other words, with the control law (8), the set $\mathcal{D}^b_\infty$ is repelling. Since $\partial\mathcal{D}^g_\infty = \mathcal{D}^b_\infty \cup \{0\}$, it also follows that $\mathcal{D}^g_\infty$ is invariant. ■

REFERENCES

[1] M. Aicardi, G. Casalino, A. Bicchi, and A. Balestrino, "Closed loop steering of unicycle-like vehicle via Lyapunov techniques," *IEEE Robot. Automat. Mag.*, vol. 2, pp. 27–35, Mar. 1995.

[2] A. Astolfi, "Discontinuous control of the nonholonomic integrator ," in *Modeling and Control of Mechanical Systems*, A. Astolfi, D. Limebeer, and A. Tornambe, Eds. London, U.K.: Imperial College, 1997, pp. 293–309.

[3] ——, "Exponential stabilization of a wheeled mobile robot via discontinuous control," *J. Dynam. Syst., Meas., Control*, vol. 121, pp. 121–126, 1999.

[4] A. Bloch and S. Drakunov, "Stabilization and tracking in the nonholonomic integrator via sliding modes," *Syst. Control Lett.*, vol. 29, pp. 91–99, 1996.

[5] C. Canudas de Wit, H. Khennouf, C. Samson, and O. J. Sørdalen, "Nonlinear control design of mobile robots," in *The Book of Mobile Robots*, Singapore: World Scientific, 1996.

[6] A. De Luca, G. Oriolo, and M. Vendittelli, "Control of wheeled mobile robots: An experimental overview," in *RAMSETTE: Articulated and Mobile Robots for SErvices and TEchnology*, S. Nicosia, B. Siciliano, A. Bicchi, and P. Valigi, Eds. London, U.K.: Springer-Verlag, 2001, vol. 270.

[7] H. K. Khalil, *Nonlinear Systems*, 2nd ed. Englewood Cliffs, NJ: Prentice-Hall, 1996.

[8] H. Khennouf and C. Canudas de Wit, "On the construction of stabilizing discontinuous controllers for nonholonomic systems," in *Proc. IFAC Nonlinear Control Syst. Design Symp.*, Tahoe City, CA, 1995, pp. 747–752.

[9] R. T. M'Closkey and R. M. Murray, "Convergence rates for nonholonomic systems in power form," in *Proc. American Control Conf.*, San Francisco, CA, 1993, pp. 467–473.

[10] ——, "Nonholonomic systems and exponential convergence: Some analysis tools," in *Proc. 32nd Conf. Decision and Control*, San Antonio, TX, 1993, pp. 943–948.

[11] ——, "Experiments in exponential stabilization of a mobile robot towing a trailer," in *Proc. American Control Conf.*, Baltimore, MD, 1994, pp. 988–993.

[12] ——, "Exponential stabilization of driftless nonlinear control systems using homogeneous feedback," *IEEE Trans. Automat. Contr.*, vol. 42, pp. 614–628, May 1997.

[13] M. R. Murray and S. S. Sastry, "Nonholonomic motion planning: Steering using sinusoids," *IEEE Trans. Automat. Contr.*, vol. 38, pp. 700–716, May 1993.

[14] L. A. Pars, *A Treatise on Analytical Dynamics*. London, U.K.: Heinemann, 1965.

[15] J. B. Pomet, "Explicit design of time-varying stabilizing control laws for a class of controllable systems without drift," *Syst. Control Lett.*, vol. 18, pp. 147–158, 1992.

[16] A. Teel, R. Murray, and C. Walsh, "Nonholonomic control systems: From steering to stabilization with sinusoids," in *Proc. 31st Conf. on Decision and Control*, Tucson, AZ, 1992, pp. 1603–1609.

[17] P. Tsiotras, "Invariant manifold techniques for control of underactuated mechanical systems," in *Modeling and Control of Mechanical Systems*, A. Astolfi, D. Limebeer, and A. Tornambe, Eds. London, U.K.: Imperial College, 1997, pp. 277–292.

[18] P. Tsiotras and J. Luo, "Reduced-effort control laws for underactuated rigid spacecraft," *J. Guid. Control Dyn.*, vol. 20, no. 6, pp. 1089–1095, 1997.

[19] ——, "Stabilization and tracking of underactuated axi-symmetric spacecraft with bounded inputs," *Automatica*, vol. 36, no. 8, pp. 1153–1169, 2000.

ByungMoon Kim received the B.S. degree in 1994 from Inha University, Incheon, Korea, and the M.S. degree in 1999 from Georgia Institute of Technology, Atlanta, where he is currently working toward the Ph.D. degree.

His current research interests are computer graphics, modeling, computer vision animation, simulation, dynamics, and control theory.

Panagiotis Tsiotras (S'90–M'92–SM'02) received the Eng. Dipl. in mechanical engineering from the National Technical University of Athens, Greece, in 1986, the M.Sc. degree in aerospace engineering from Virginia Polytechnic Institute and State University, Blacksburg, in 1987, and the M.Sc. degree in mathematics and the Ph.D. degree in aeronautics and astronautics from Purdue University, West Lafayette, IN, in 1992 and 1993, respectively.

He was an Assistant Professor with the Department of Mechanical and Aerospace Engineering, University of Virginia, Charlottesville, from 1994 to 1998. Since September 1998, he has been an Associate Professor in the School of Aerospace Engineering, Georgia Institute of Technology, Atlanta, and the Director of the Dynamics and Controls Systems Laboratory (DCSL) in the same department. He is an Associate Editor of the *AIAA Journal of Guidance, Control, and Dynamics*, and *Dynamics and Control*. His current research interests include dynamics and control of nonlinear systems, optimal and robust control, with applications to mechanical and aerospace systems.